Safety of intracranial electroencephalography during functional electromagnetic resonance imaging in humans at 1.5 tesla using a head transmit RF coil: Histopathological and heat-shock immunohistochemistry observations

Joan Y.W. Liu [a,b,c,1], Hassan B. Hawsawi [a,d,1,*], Niraj Sharma [a], David W. Carmichael [e,f], Beate Diehl [a,g], Maria Thom [a,b], Louis Lemieux [a]

[a] Department of Clinical and Experimental Epilepsy, UCL Queen Square Institute of Neurology, Queen Square, London WC1N 3BG, United Kingdom
[b] Division of Neuropathology, National Hospital of Neurology and Neurosurgery, Queen Square, London WC1N 3BG, United Kingdom
[c] School of Life Sciences, University of Westminster, London W1W 6UW, United Kingdom
[d] Administration of Medical Physics, King Abdullah Medical City (KAMC), Makkah, Saudi Arabia
[e] Developmental Imaging and Biophysics Section, UCL Great Ormond Street Institute of Child Health, London, United Kingdom
[f] Wellcome EPSRC Centre for Medical Engineering, King's College London, St Thomas' Hospital, London, United Kingdom
[g] National Hospital of Neurology and Neurosurgery, Queen Square, London WC1N 3BG, United Kingdom

ARTICLE INFO

ABSTRACT

Objectives: Simultaneous intracranial EEG and functional MRI (icEEG-fMRI) recordings in humans, whereby EEG is recorded from electrodes implanted inside the cranium during fMRI scanning, were made possible following safety studies on test phantoms and our specification of a rigorous data acquisition protocol. In parallel with this work, other investigations in our laboratory revealed the damage caused by the EEG electrode implantation procedure at the cellular level.

The purpose of this report is to further explore the safety of performing MRI, including simultaneous icEEG-fMRI data acquisitions, in the presence of implanted intra-cranial EEG electrodes, by presenting some histopathological and heat-shock immunopositive labeling observations in surgical tissue samples from patients who underwent the scanning procedure.

Methods: We performed histopathology and heat shock protein expression analyses on surgical tissue samples from nine patients who had been implanted with icEEG electrodes. Three patients underwent icEEG-fMRI and structural MRI (sMRI); three underwent sMRI only, all at similar time points after icEEG implantation; and three who did not undergo functional or sMRI with icEEG electrodes.

Results: The histopathological findings from the three patients who underwent icEEG-fMRI were similar to those who did not, in that they showed no evidence of additional damage in the vicinity of the electrodes, compared to cases who had no MRI with implanted icEEG electrodes. This finding was similar to our observations in patients who only underwent sMRI with implanted icEEG electrodes.

Conclusion: This work provides unique evidence on the safety of functional MRI in the presence of implanted EEG electrodes. In the cases studied, icEEG-fMRI performed in accordance with our protocol based on low-SAR (≤0.1 W/kg) sequences at 1.5T using a head-transmit RF coil, did not result in measurable additional damage to the brain tissue in the vicinity of implanted electrodes. Furthermore, while one cannot generalize the results of this study beyond the specific electrode implantation and scanning conditions described herein, we submit that our approach is a useful framework for the post-hoc safety assessment of MR scanning with brain implants.

---

* Corresponding author at: Department of Clinical and Experimental Epilepsy, UCL Queen Square Institute of Neurology, Queen Square, London WC1N 3BG, United Kingdom.

E-mail address: hassan.hawsawi.15@ucl.ac.uk (H.B. Hawsawi).

[1] These authors contributed equally to this work.

1. Introduction

Electroencephalography (EEG) is an important technique capable of recording electrical brain activity in patients. Intracranial electroencephalography (icEEG) plays a significant role in the evaluation and planning for the surgery in some patients with drug-resistant epilepsy, and is considered the gold standard for the localization of the epileptic zone and the surrounding activity with higher sensitivity and spatial resolution than scalp EEG (Murta et al., 2014; Vulliemoz et al., 2010). There are three types of icEEG electrodes: depths, which consist of 1 mm diameter probes with regularly spaced ring-shaped metallic recording contacts placed within the brain; and subdural grids and strips, which consist of planar arrays (a single row for strips) of regularly-spaced metallic disk-shaped contacts imbedded in a silicon sheet and placed on brain's surface. Depth EEG recording electrodes are similar in design, diameter and materials to those used for deep brain stimulation (DBS) in movement disorders and other conditions (Hawsawi et al., 2017). When appropriate and possible, based on the results of non-invasive imaging, electrophysiological and clinical evaluations, icEEG offers greater sensitivity and enhanced localizing value for ictal epileptic activities than scalp EEG (Jayakar et al., 2016; Tao et al., 2005). Because of its very localized sensitivity profile, particularly in the case of depth electrodes, icEEG requires the use of multiple implants, an invasive surgical procedure associated with risks of infection, headache, intracerebral hemorrhage, neurological deficit, fever, nausea, and infarction (Gonzalez-Martinez et al., 2015; Koubeissi et al., 2009; Yan et al., 2019). The degree of those complications is attributed to several factors including the number of electrode implants, the types and (material) composition of electrodes, the age of the subject and the location of the insertion of the icEEG implants (Enatsu and Mikuni, 2016). The resulting spatial sampling is an important limitation of icEEG which may be mitigated by combining it with a non-invasive technique such as functional magnetic resonance imaging (fMRI) (Vulliemoz et al., 2011).

Functional Magnetic resonance imaging (fMRI) with simultaneous EEG recording, is a powerful technique because of its ability to map blood oxygenation level dependent (BOLD) signals related to events or states observed on the latter (Glynn and Detre, 2013; Goebel and Esposito, 2010). In patients with epilepsy, this technique may help to develop better surgical strategies (Gonzalez-Martinez et al., 2015) and, more specifically localize the BOLD changes associated with interictal (Vulliemoz et al., 2011) and ictal discharges (Chaudhary et al., 2016). EEG-fMRI has been used to reveal interictal epileptiform discharge-related BOLD networks which may be used during pre-surgical planning to improve postsurgical outcome (An et al., 2013; Centeno et al., 2017; Coan et al., 2016; Oya et al., 2017; Thornton et al., 2010). Simultaneous icEEG-fMRI, a more recent development, adds the potential advantage of much greater electrophysiological sensitivity to fMRI's whole-brain mapping capability (Carmichael et al., 2010; Chaudhary et al., 2016; Cunningham et al., 2012; Murta et al., 2017; Ridley et al., 2017; Vulliemoz et al., 2011).

The acquisition of any type of MRI data requires excitation of the brain using radiofrequency signals (Deichmann, 2016), leading to temperature increases (Angelone et al., 2006, 2004; Carmichael et al., 2010). According to the international safety guidelines, the temperature of the human tissue in moderate environmental conditions (ambient temperature more than 25 °C and relative humidity above 60%) (MHRA, 2015) should not be increased by more 1 °C and 3.2 W Kg $^{-1}$ for the head-average over an exposure of 6 min (IEC, 2016). Furthermore, heat-related tissue damage is a function of exposure time (Sapareto and Dewey, 1984).

In the presence of metallic, conductive devices such as icEEG electrodes, additional hazards might arise in the vicinity of the electrodes due to the interaction between the scanner-generated radio-frequency (RF) electromagnetic (EM) waves and the electrodes' metallic components: antenna effects (Carmichael et al., 2010, 2007; Golestanirad et al., 2019, 2017a, 2017b). This mechanism can give rise to excessive local current concentrations with resulting tissue burns. In addition, the scanner gradients with switching frequencies in the kHz range can induce currents in loops formed by the electrodes and human tissue, resulting in possible localized heating (Lemieux et al., 1997). For neurological implants, the recommended maximum temperature increase is 2 °C ((ANSI-AAMI-ISO-14708, 2012); see (Serano et al., 2015)).

We have previously performed experiments in test phantoms in 1.5 T and 3 T MRI scanners and to assess the likely increases in temperature in the vicinity of implanted depth electrodes. We found that when using a fast spin echo sequence, such as used for structural MR imaging, the temperature increase was in the range +0.3–1 °C when the head RF transmit coil was used in a 1.5 T MRI scanner for a range of circuit configurations and temperature increases of up to 6.9 °C in the 3 T scanner using the body RF transmit coil, highlighting the need for careful safety testing and detailed, restrictive scanning implementation protocols (Carmichael et al., 2012, 2010). We concluded that temperature elevation can be kept within the safe limits (below 1 °C) by using MRI head transmit coil, applying less SAR sequences, and positioning the EEG cables along the central z-axis with the open circuit configuration rather than the short circuit (Carmichael et al., 2010). In accordance with guidance (U.S. Food and Drug Administration US-FDA, 2021) for 'off-label' research use of medical devices, this evidence was used to obtain local ethical committee approval allowing us to perform simultaneous icEEG-fMRI investigations into human epileptic activity (Murta et al., 2017, 2016; Ridley et al., 2017; Vulliemoz et al., 2011), without incident or discomfort reported by the patients.

However, the phantom studies we performed, and the feedback obtained from the patients who subsequently underwent icEEG-fMRI at our center (and the clinicians involved in their management), while reassuring do not provide a complete picture of the technique's safety. In particular, it is possible that asymptomatic brain damage has taken place that could be revealed by histopathological examinations (Coffey et al., 2014). Therefore, we wanted to obtain more direct, *a posteriori* evidence on the effect of MR scanning while recording icEEG on the human brain for the first time ever (to our knowledge) taking advantage of the local expertise in the application of histopathology to the study of post-implantation brain damage (Goc et al., 2014).

In this paper, we report the results of histopathological analysis of tissue in the vicinity of the icEEG depth electrode implantation in three patients who underwent icEEG-fMRI and compared with histopathological data from three patients that underwent structural MRI only at a similar time point following icEEG electrode implantation. We also interpret the findings in relation to a larger study on the damage caused by the implantation process itself, without exposure to fMRI (Goc et al., 2014). Additionally, the expression of heat shock proteins, which are upregulated in cells in response to stress, such as thermal changes or injuries, and can activate immune responses through inducing the synthesis of pro-inflammatory cytokines and promoting the maturation of lymphocytes and dendritic cells (Van Eden et al., 2005), was investigated to further study RF-related heating damage around penetrating lesions.

2. Materials and methods

Nineteen patients with severe epilepsy underwent simultaneous icEEG-fMRI scans for research purposes at the end of their clinical invasive EEG investigations. All patients in whom histopathology along the implanted depth electrodes' paths was available were selected for this study. Three out of the 19 patients met this criterion: Cases Goc-7 and Goc-10 (histopathology results were previously reported (Goc et al., 2014), and case NEW-1 (histopathology not previously reported). These patients also underwent structural MRI (sMRI) with implanted icEEG electrodes for clinical (implantation localization verification, performed immediately after implantation) purposes.

In addition, six patients who did not undergo simultaneous icEEG-fMRI scanning were included in the study as controls: three who

Table 1
Imaging, clinical details and HSP60 test status of cases.

Case	Age at surgery (years) / gender	Implanted icEEG electrodes (lobe)*	MR imaging		Age (DPI) and type of electrode-related lesion	Location of resection	Underlying pathology	HSP-60 test performed?
			Simultaneous icEEG-fMRI?	Structural MRI with implanted icEEG electrodes?				
Goc-7	34/F	2 depths (F) 2 grids (F) 2 strips (F)	Yes	Yes	10 ET	Frontal cortex	FCD IIB	Yes
Goc-10	29/M	2 depths (F) 2 grids (F, P-T)	Yes	Yes	13 SG	Frontal cortex	FCD IIB	Yes
New-1	45/M	2 depths (T) 2 grids (T-F, T)	Yes	Yes	461 ET	Temporal white matter	LGG (WG I)	No
Goc-5	23/F	2 depths (T) 1 grid (T) 1 strip (T)	No	Yes	10 ET	Temporal cortex	-	Yes
Goc-17	34/M	4 depths (T) 1 strip (F)	No	Yes	301 ET	Temporal white matter	HS and old contusions	Yes
New-2	55/M	4 depths (T) 2 grids (T) 2 strips (F)	No	Yes	385 ET	Temporal	-	No
Goc-15	52/M	1 depth (F) 1 grid (F) 1 strip (P)	No	No	209 ET	Frontal white matter	FCD IIB	Yes
New-3	49/M	2 grids (F) 2 strips (F)	No	No	3 SG	Frontal cortex	DNT	Yes
New-4	23/F	2 depths (F) 2 grids (F) 2 strips (F-P)	No	No	6 ET	Frontal cortex	-	Yes

The cases are stratified into three sub-groups defined based on the combination of types of, or absence of, MRI imaging in the presence of implanted icEEG electrodes. The age of icEEG lesion in each case was recorded as number of days post injury (DPI; interval between electrode implantation and tissue resection). The area of icEEG lesions ranged from 0.69 to 2.81mm^2 (average$\pm$$S$.E.M., 1.57mm^2$\pm$0.30). Tissue samples were not available for HSP60 labeling for cases New-1 and New-2. * Underlined: tissue-sample electrode(s).
F: Frontal; T: Temporal; P: Parietal. DNT: Dysembryoplastic neuroepithelial tumor; ET: Electrode track; FCD: Focal Cortical Dysplasia; HS: Hippocampal sclerosis; LGG: Low grade glioneuronal tumor; SG: Subdural grid lesion; -: No significant pathology. WG: WHO Grade.

underwent sMRI with implanted icEEG electrodes: Goc-5 and Goc-17 (histopathology results previously reported (Goc et al., 2014)), and NEW-2 (not previously reported); and three who had no sMRI with implanted icEEG electrodes: Goc-15 (histopathology results previously reported (Goc et al., 2014)), NEW-3 and NEW-4 (not previously reported).

In summary, we have three groups of three cases each, characterized as: icEEG-fMRI and sMRI; sMRI only; and no sMRI or icEEG-fMRI (Table 1). The details of each patient's icEEG electrode implantation are contained in the Appendix. In summary, in 8/9 cases the implantation comprised a mixture of depth and subdural (grid or strip) electrodes, and one case had subdural grids and strips only. The number of implanted electrodes ranged from 3 to 8 (mean: 4.9), of which between 0 and 4 were depth electrodes (mean: 2.1), and 1 and 4 were subdural grids and strips (mean: 2.8). The mean number of implanted electrodes for the groups ranged from 4.3 to 5.7. The targeted lobes were: temporal (6 cases), frontal (8 cases) and parietal (3 cases). The ages of the electrode lesions (interval between icEEG investigation and surgical resection) ranged from a few days to more than a year in all three groups. See Table 1.

2.1. Simultaneous icEEG-fMRI research scans (patients: Goc-7, Goc-10 and NEW-1)

At the end of the invasive EEG monitoring period, the patients were disconnected from the clinical recording system and taken to the neuroradiology department to undergo a simultaneous icEEG-fMRI data acquisition as part of a research project on the generators of epileptic ac-

tivity approved by the joint UCL/UCLH ethical review committee. The patients gave written, informed consent to participate in the research.

The patients were scanned using a 1.5T Avanto scanner (Siemens, Erlangen, Germany) with the head transmit and receive radiofrequency (RF) coil in accordance with our protocol (Carmichael et al., 2010).

For patients Goc-10 and NEW-1, all implanted electrodes were recorded from during fMRI acquisitions. These were connected to the MR-compatible amplifiers (BrainAmp MR Plus, Brain Products, Munich, Germany) using short cables (90 cm long) specifically for the icEEG-fMRI scanning session, in accordance with our protocol (Carmichael et al., 2012, 2010). For patient Goc-7, due to the limited number of recording channels of the MR-compatible amplifiers, the recordings during fMRI were limited to the following electrodes: the two left frontal subdural grids (('G1-01 to G1-64′) and ('G2-01 to G2-16′)) and two depth electrodes (('DA01-DA06') and ('DP01-DP06')).

The icEEG-fMRI scanning protocol consists of:

(1) Localizer, (2) FLASH T1-volume (TR 3 s, TE 40 ms, flip angle 90° and Specific Absorption Rate (SAR): 0.1 W/Kg head average), (3) two 10 min gradient echo EPI fMRI scans (TR 3 s, TE 78 ms, 38 slices, 200 vol $3 \times 3 \times 3$ mm, and SAR: 0.1 W/Kg head average) for Goc-7, three 10 min gradient echo EPI fMRI scans (TR 3 s, TE 78 ms, 38 slices, 200 vol $3 \times 3 \times 3$ mm, and SAR: 0.2 W/Kg head average) for Goc-10, two 10 min gradient echo EPI fMRI scans (TR 3 s, TE 40 ms, 38 slices, 200 vol $3 \times 3 \times 3$ mm, and SAR: 0.2 W/Kg head average), and two 10 min gradient echo field mapping three 10 min gradient echo EPI fMRI scans (TR 0.8 s, TE 4.92 ms, 38 slices, 200 vol $3 \times 3 \times 3$ mm, and SAR: 0.1 W/Kg head average) for NEW-1.

Table 2

Protocol for immunohistochemical study.

Antibody (source)	Epitope/labeling pattern in normal cortex	Pre-treatment, Antibody dilution (mins, temperature)
NeuN (EMD)	Neuronal nuclear antigen/neuronal nuclei and cytoplasm	ER1, 1:2000 (20, RT)
SMI32/31 (Sternberger)	Neurofilament (non-photosphorylated and phosphorylated 200 kDa proteins)	1:500 (20, RT)
GFAP (DAKO)	GFAP/astrocytes	ENZ1, 1:2500 (20, RT)
SIM94 (Sternberger)	Myelin basic protein	ENZ1, 1:2000 (20, RT)
Iba1 (Wako)	Ionized calcium binding adaptor molecule 1 protein expressed in macrophage and microglia	H-3300, 1:1000 (ov, 40 °C)
CD34 (DKAO)	Stem cell marker/endothelial cells, glioma	1:50 (20, RT)
Nestin (Abcam)	Intermediate filament; developmentally regulated/expressed in stem cells and radial glial	H-3300, 1:1000 (ov, 4 °C)

Antigen retrieval buffers (buffers used in auto-immunostainer is in italics): *ENZ1*, Bond enzyme concentrate and diluent (Leica, Milton Keynes, UK); *ER1*, Bond citrate-based buffer (Leica, Milton Keynes, UK); H-3300 Vector's citrate-based buffer pH6.0 (Vector Lab, Peterborough, UK). Suppliers: EMD Millipore, Watford, UK; Sternberger, Maryland, US; DAKO, Cambridgeshire, UK; Abcam, Cambridge, UK; FUJIFILM Wako Pure Chemical Corporation, Osaka, Japan. RT: room temperature; ov: overnight.

2.2. Structural MRI scans for implantation localization verification (patients: Goc-7, Goc-10, NEW-1, Goc-5, Goc-17 and NEW-2)

As part of the clinical invasive EEG monitoring protocol all patients should undergo a sMRI scanning protocol, using the same 1.5T Avanto MRI scanner, to verify the position of the implanted electrodes which consists of: 1) Localizer, 2) T1-weighted magnetization-prepared rapid (MPR) gradient echo volume (TR 1930 ms, TE 3.37 ms, TI 1100 ms, flip angle 15° and SAR: 0.1 W/Kg head average).

This protocol is not performed in some patients in certain circumstances, such as the icEEG electrodes being too close together as determined by intra-operative X-ray; this was the case for Goc-15, NEW-3 and NEW-4.

2.3. Histopathology samples

Surgically resected tissue from all cases was retrieved from the Epilepsy Society Brain and Tissue Bank at UCL Queen Square Institute of Neurology, Division of Neuropathology, UK, and written consents were obtained from patients prior to the use of tissue for research. Patients underwent frontal or temporal lobectomy at National Hospital for Neurology and Neurosurgery (London, UK) as treatment for their refractory epilepsy. Clinical details including the time interval between icEEG recording and surgical resection are summarized in Table 1. Immediately after surgery, surgical tissue was fixed in 10% neutral-buffered formalin, and was macroscopically dissected into 5 mm-thick blocks. Tissue blocks were then processed through graded alcohol and xylene before embedding in paraffin wax. Paraffin-embedded blocks were sectioned at 5 μm (or 14 μm for histological staining) on a microtome (Leica, UK). For neuropathological assessment, sections from each case were routinely stained using Hematoxylin and Eosin (H&E), Luxol Fast Blue (LFB), and immunolabelled using neuronal (NeuN, SMI31, SMI32), astroglia (GFAP), microglia (iba1), myelin (SMI94R), endothelial (CD34) and immature cell markers (Nestin) following established protocols as previously described (Goc et al., 2014) (see Table 2). Images of sections were acquired using a brightfield microscope connected to a camera (Zeiss Axio Imager 2, Germany).

In addition, immunohistochemistry using antibodies against heat shock protein 60 (HSP60; 1:1000; Cell Signal Technology, UK) were performed on seven cases: Goc-7 and Goc-10 (icEEG-fMRI), Goc-5 and Goc-17 (sMRI and implanted icEEG), Goc-15, NEW-3 and NEW-4 (icEEG only). Tissue samples from NEW-1 and NEW-2 were not available for this analysis. Three zones were defined for this analysis in relation to the position of the injury caused by each electrode: zone 1 (immediate vicinity: 0–350 μm), zone 2 (350–700 μm) and zone 3 (remote ≥2000 μm) as previously described (Goc et al., 2014).

For quantitative analysis, HSP60-immunolabelled sections were scanned at 20x magnification using the whole-slide scanner, AxioScan.Z1 (Zeiss, Germany) and scans were analysed using the image analysis software, QuPath (Bankhead et al., 2017). For each scan, zone 1, 2 and 3 were annotated at 2x magnification using the same method

as previously described in (Goc et al., 2014). In brief, the internal border of zone 1 outlined the periphery of the lesion core and the outer border of zone 1 was 350 μm away from the internal border thus forming a circumferential region surrounding the lesion. The internal border of zone 2 followed the outer border of zone 1 and its outer border was 350 μm distanced from the internal border of zone 2. The control region of <2000 μm2, zone 3, was sampled as far away from the lesion as possible within normal-appearing tissue in the same tissue section. For automated quantification, QuPath was trained to recognize immunopositive labeling within the tissue section using the positive labeling detection module in QuPath where DAB threshold (positive) was set at 0.08 OD unit and haematoxylin threshold was set to 0.1 OD unit. The percentage area of HSP60-positive immunolabelling per zone were compared amongst three zones per case and amongst groups. Statistical tests including Krusal-Wallis and Spearman correlations were performed using SPSS (v24; IBM, USA; $P < 0.05$) to compare the percentage area of HSP60-immunopositive labeling amongst zones for each case, and to examine the relationship between percentage area of HSP60-immunopositive labeling and the age of lesion (days post-lesion).

3. Results

None of the patients who underwent icEEG-fMRI reported any discomfort during or following the scan.

Electrode penetrating lesions were identified in all cases during neuropathological assessment of the cases with depth electrodes; we note that the portion of the penetrating lesion length contained in the samples varies from a cross-section to a significant length, depending on their relative orientation. Except for case Goc-7, the penetrating lesions studied here were in areas away from any epilepsy pathology. Noting that the lesion tracts can only be identified microscopically with confidence after histological/immunohistochemical staining, the gross appearance of the tissue samples was similar to other epileptic tissue specimens; The same observation applies to the samples from tissue adjacent to subdural grids.

3.1. Pathology relating to epilepsy

H&E and LFB stained sections showed abnormal cortical lamination and myeloarchitecture in the frontal cortex of cases Goc-7 and Goc-10. Dysmorphic neurons immunopositive for SMI31 and SMI32, and balloon cells immunopositive for CD34, Nestin, and GFAP were also observed, mainly at the gray/ white matter border. Dysmorphic neurons and balloon cells are typically observed in the brains of patients with focal cortical dysplasia type IIB (ILAE classification system) (Blümcke et al., 2011). The temporal cortex of case NEW-1 appeared normal, except for the superior temporal gyrus, which was strongly immunopositive for GFAP and showed enlarged SMI32 immunopositive neurons and vacuolation of the parenchyma. Infiltration of inflammatory cells, including microglia was also noted. No marked neuronal loss was observed in the hippocampus. Tissue from the lesion sample showed patchy immunoreactivity with BRAF V600, low numbers of Ki67 immunopositive cells,

but the presence of many angular cells and large dysmorphic neurons. The lesion was negative for IDH1(R132H). Case NEW-1 was likely to show pathology consistent with a low grade glioneuronal tumor (WHO grade 1).

3.2. Pathology relating to intracranial electrode insertion

The pathologies around intracranial electrode insertion sites observed in cases Goc-7, Goc-10 and NEW-1 were not remarkably different from controls (Goc-5, Goc-15, Goc-17, NEW-2, NEW-3 and NEW-4) or other epilepsy cases who did not undergo simultaneous icEEG-fMRI (Goc et al., 2014). Surgical tissue from all patients showed microscopic focal lesions characteristic of injury caused by intracranial subdural or depth electrodes during icEEG.

Focusing on the three cases who underwent simultaneous icEEG-fMRI, the lesion in case Goc-7 was located deeply in the gray and white matter demarcation, while the lesion in case Goc-10 was noted superficially in the cortex. The lesion in case NEW-1 was found in the white matter of the hippocampus. For cases Goc-7, and Goc-10, the lesions were estimated to be between ten to 13 days old (post icEEG). Lesions in both cases Goc-7 (Figs. 1A,B) and Goc-10 (Figs. 2A,B) had a necrotic core, infiltrated by numerous inflammatory cells including macrophages, microglia and lymphocytes which is characteristic of an acute inflammatory response. Increased cellularity was also observed in the regions immediately around the lesion core (zone 1) and extending to nearby 'normal-appearing' regions of the tissue. The lesion core in case Goc-10 had the appearance of acellular coagulative necrosis, and the deposition of fibrous materials that appeared to be strongly eosinophilic on H&E stained sections (Fig. 2A).

Many iba1-immunopositive microglia and activated macrophages were observed in the lesion core and immediate periphery of case Goc-7 (Fig. 1C). Most iba-1 immunopositive cells in this region were enlarged and intensely labelled, and appeared to form focal clusters or aggregates (Fig. 1D). Nestin immunoreactivity was observed around the necrotic core (Fig. 1E). Thick, short 'strapped-like' nestin immunopositive fibres and cells were observed in the penumbra of the lesion (Fig. 1F). Endothelial cells in blood vessels around the lesion were also intensely expressing nestin and CD34. Compared to iba1 and nestin immunoreactivities in zone 1, the expression of GFAP astrocytic processes and soma was observed further away from the lesion core in zone 2. The necrotic core and its immediate vicinity was generally immunonegative for GFAP in case Goc-7 (Fig. 2C). GFAP immunopositive cells in zone 2 were multipolar and heterogenous in size. Intensely-labelled GFAP immunopositive processes and cells were observed perivascularly along the length of blood vessels (Fig. 2D). The lesion observed in case NEW-1 had the appearance of a chronic fibrous scar composed of eosinophilic collagen fibres. The lesion was estimated to be over year and three months. Inflammatory mediators were still numerous and visible in the lesion. Similar changes to cellularity and inflammatory reactions were also observed in the vicinity of the electrode placement sites in control cases.

3.3. Heat shock protein 60 (HSP60)-immunopositive labeling

The distance between the centres of zones 1 and 3 was in the range 8.1 to 14.0 mm along the x-axis (average ± S.E.M: 10.3 ± 0.7 mm) and 2.4 to 7.6 mm along the y-axis (4.3 ± 0.6 mm).

In the seven cases studied for heat-related damage, HSP60 immunopositive labeling was predominantly observed in the cerebral cortex, particularly in layer I or subpial layer (Fig. 3A), and perivascular regions (Fig. 3B). In these areas, HSP60 immunolabelling appeared to be granular, and clustered in the parenchyma and/or perinuclear regions within cells (Fig. 3B). HSP60 immunopositive labeling was also observed in regions around penetrating injuries caused by icEEG electrode placement (Figs. 4A–C, E–G). Intensely immunolabelled neuronal and glial-like cells as well as endothelial cells were observed near penetrating injuries (zones 1 and 2) in all cases (Figs. 4B,C,F–G). Quanti-

tative analysis of HSP60 immunopositive labeling in all cases revealed significantly higher percentage of HSP60 immunolabelling in zones 1 and 2 than in the remote region, zone 3 ($p = 0.006$, $p = 0.042$, respectively; non-parametric Kruskal-Wallis test; Fig. 5). No significant correlation was observed between the percentage of HSP60 immunolabelling in each zone and days after injury ($P > 0.05$). Qualitatively, no marked difference in HSP60 immunolabelling was observed in any of the zones between the cases that underwent simultaneous icEEG-fMRI than controls.

4. Discussion and conclusions

The combination of the clinical and scientific importance of MRI and increased use of brain implants in patients with neuronal diseases raises the level of interest in the safety aspects of performing MRI in the presence of invasive devices (Erhardt et al., 2018). We investigated the possibility of additional cellular damage caused specifically by exposure of the brain to the radio-frequency electromagnetic waves used in MRI scanning in the presence of indwelling metallic implants, namely intracranial EEG electrodes (depth, and subdural grids and strips) used for the pre-surgical evaluation of patients with severe epilepsy. In this retrospective study we examined tissue from surgical samples in a group of patients who took part in a research project focused on mapping the changes in blood flow associated with epileptic discharges recorded invasively as measured using functional MRI (Carmichael et al., 2012; Chaudhary et al., 2016; Murta et al., 2016; Vulliemoz et al., 2011).

In summary, we found that the pathology observed in three patients who had undergone simultaneous icEEG-fMRI for research purposes was not remarkably different from other epilepsy cases who had not undergone icEEG-fMRI, or not undergone any MRI with implanted icEEG electrodes (as performed as part of our clinical procedure for localization purposes), in line with our previous findings (Goc et al., 2014; Liu et al., 2012; Stephan et al., 2001). These results also provide new histopathological evidence on the risks associated with performing sMRI for icEEG electrode localization verification. Namely, that the findings for the three cases in the sub-group who underwent sMRI only were unremarkable (same inflammatory reactions) compared to those who did not undergo any MRI with icEEG electrodes.

Up to now, the safety of MR scanning in the presence of intracranial leads, and in particular the issue of RF-induced heating, has been investigated prospectively (i.e. prior to application in living subjects) mostly using two methodologies: temperature measurements in test objects (gel phantoms and animal cadavers) and computational simulations. Such studies, such our own in gel phantoms (Carmichael et al., 2010, 2008), are typically performed in advance of MR scanning of human subjects with the implants to obtain evidence on the level of risk posed by the scanning. This evidence can then be used to establish the feasibility and conditions under which application in humans can be performed with an acceptable risk level, as was done in advance of the acquisition of the MRI data considered in the present work (Carmichael et al., 2012). In addition, there have been retrospective reviews aimed at identifying complications resulting from MR scanning of patients with implants for clinical purposes (Davis et al., 1999; Erhardt et al., 2018; Larson et al., 2008; Nazzaro et al., 2010; Weise et al., 2010; Zrinzo et al., 2011). For deep brain stimulation (DBS) and recording electrodes of the type studied here, those have shown a very low rate of adverse incidents. The present study is in line with this approach, but focused on histopathological findings, by capitalizing on an ongoing investigation at our institution on brain damage caused by implantations (notwithstanding MR scanning). The retrospective study of tissue samples as performed here, is complementary to, and we suggest may even be more sensitive to certain forms of tissue damage due to localised heating, than clinical and radiological evaluations.

The sMRI and icEEG-MRI scans took place at the start and the end of each patient's clinical icEEG investigation (implantation and monitoring), respectively. Most of the implantations considered here con-
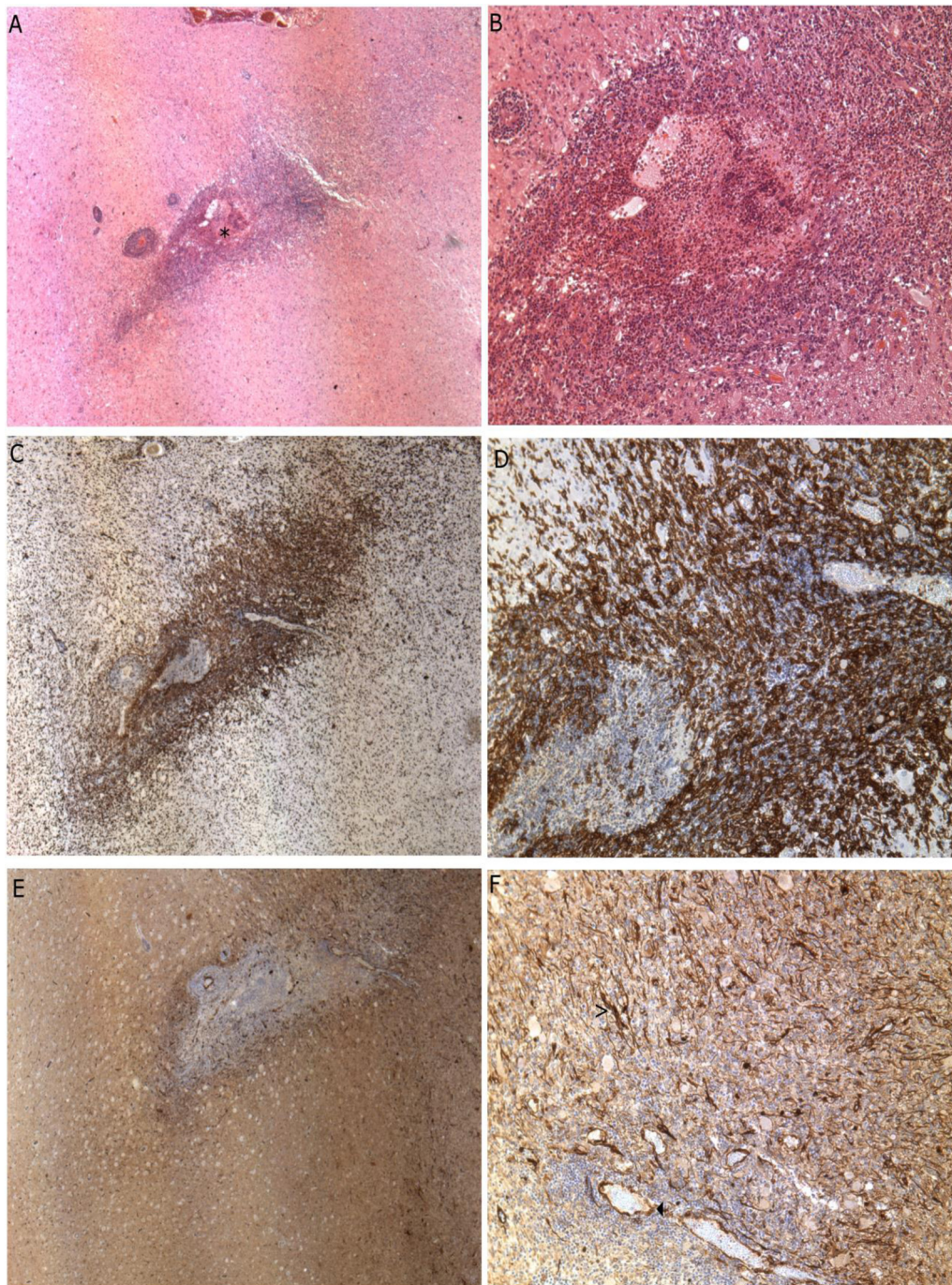
Fig. 1. Case Goc-7 with a focal lesion caused by icEEG electrode insertion. (A,B) Images of a hematoxylin and eosin stained section showing a lesion with a necrotic core and a small cavity (*) acquired at low and high magnification, respectively. The lesion was infiltrated by many small inflammatory cells. Numerous hemorrhagic blood vessels were also noted in the periphery of the lesion. (C,D) The lesion core and immediate vicinity (zone 1) were strongly immunopositive for iba1. Iba1immunopositive cells were densely populated around the lesion core. Iba1 immunopositive cells were also visible further away from the lesion. (E,F) In comparison to iba1 immunolabelling, nestin immunoreactivity was primarily observed in zone 1. Nestin immunopositive cells appeared small with multipolar processes, although occasionally bipolar cells were observed. Nestin immunopositive fibres were generally short and thick (arrowhead). Nestin immunopositive vessels could also be observed (closed arrowhead).

sisted of mixed depth and subdural electrodes, with an average of 4.9 implanted electrodes. We note that in terms of the types and number of electrodes, these correspond well to the configurations tested in our phantom work (Carmichael et al., 2010, 2008). While it is suspected that the risk associated with MR scanning of patients with brain implants is a function of the implantation configuration (i.e. the number and position and orientation of the electrodes), no systematic study of

this effect has been published to date. Furthermore, it is difficult to assess how representative of our implantations are of the wider practice as detailed descriptions of icEEG electrode implantations for epilepsy are not available in the literature, and we hope that this report will provide some impetus in this regard. Given these limitations, icEEG-fMRI is performed at our center following a strict protocol (Carmichael et al., 2012), and in particular no MRI (of any kind) can be performed in cases
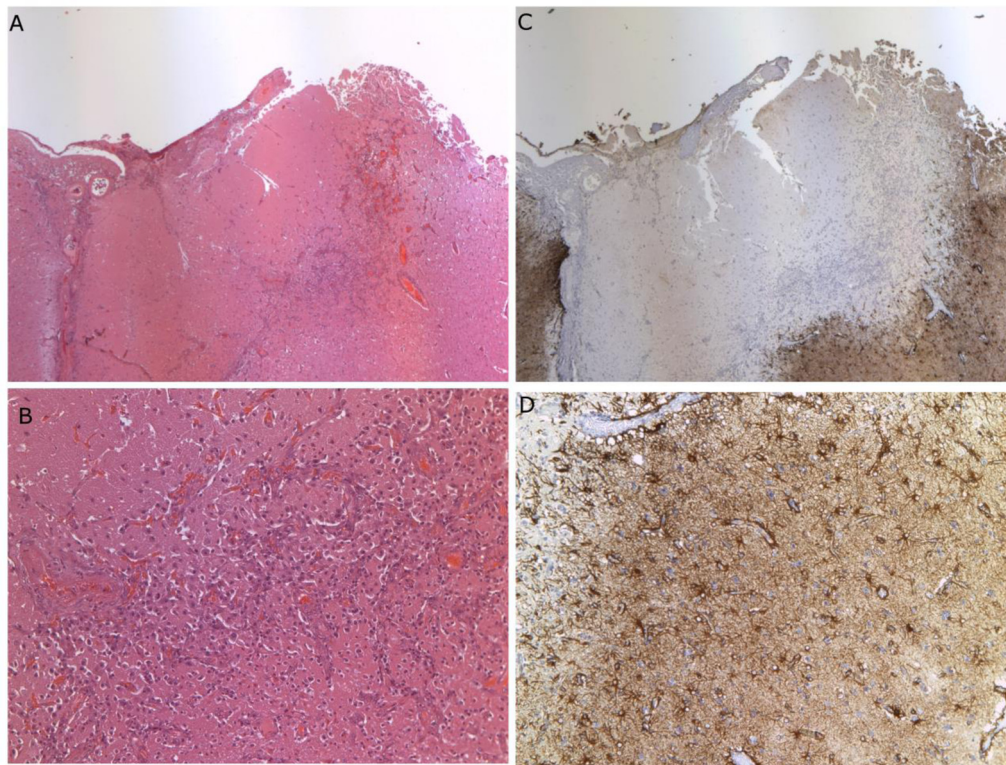
Fig. 2. Case Goc-10 with icEEG- electrode penetration-related lesion in the superficial cortex. (A,B) The lesion core in case Goc-10 had the appearance of an acellular coagulative scar. The coagulation was surrounded by irregular blood vessels (some hemorrhagic filled with red blood cells) and numerous inflammatory mediators including iba1-immunopositive microglia and macrophages. (C,D) The lesion core and its immediate vicinity was immunonegative for GFAP, but a dense matrix of GFAP immunopositive fibres were observed in zone 2, areas distanced from zone 1 of the lesion. GFAP immunopositive cells were astrocytes-like with a small cell body and multipolar processes.
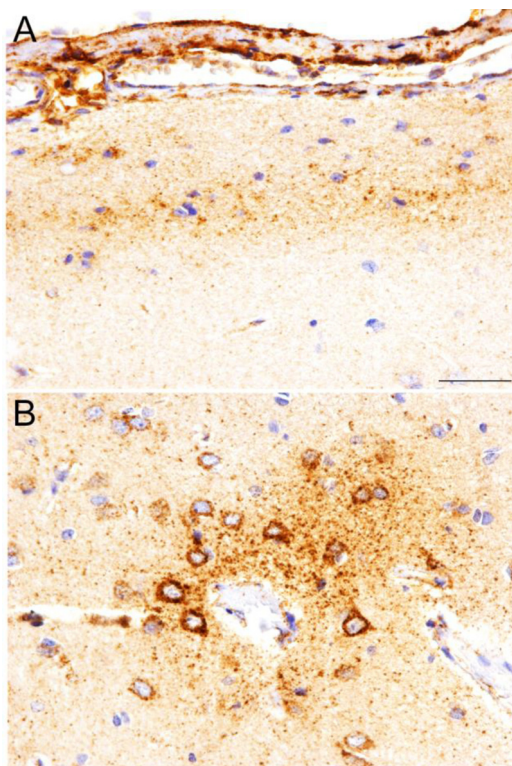

Fig. 3. HSP60 immunopositive labeling. Patient Goc-10 underwent simultaneous icEEG-fMRI and structural MRI with icEEG electrodes implanted in the frontal cortex. (A): Subpial area; (B): Perivascular area. Scale: 50 μm.

with electrodes found, or suspected, to be in contact with each other based on a post-implantation X-ray or CT. Furthermore, this research project is the subject of a prospective safety monitoring program, as part of which we request that the surgeons, when proceeding to respective surgery in cases with subdural strips and grids, to carefully examine the visual aspect of the surface of the cortex for any sign of additional damage around the electrodes and leads, such as discolouration. The patients' general neurological condition is monitored for any sign of adverse effects potentially associated with the research scan. Up to now, with 19 patients having undergone icEEG-fMRI, no such adverse effect has been observed. As a further step in this monitoring process, and following our previous work on the effects of icEEG electrode implantation (Goc et al., 2014), we wanted to examine the possibility of any effect specific to fMRI scanning in presence of indwelling icEEG electrodes at the cellular level. Three of 19 patients satisfied the selection criteria and were included in the present study.

In this study, a number of immunohistochemical markers were used to examine neuronal cell loss (NeuN, SMI31/32) and myelin changes (SMI94), vascular damage (CD34) and inflammatory response (astrogliosis (GFAP), microgliosis (Iba1) and immature cell/pericyte stimulation (Nestin)) around the vicinity of the lesion (see Table 2 and Methods Page 13 L38-42). The pathological changes around vicinity of the lesion as detected by immunohistochemistry were typical and as expected of injuries caused by invasive depth electrode placement as reported in our previous studies (Goc et al., 2014; Reeves et al., 2019) as well as by other researchers (Fong et al., 2012). We did not observe any additional pathologies around penetrating lesions in brain resections from patients who underwent simultaneous pre-surgical MRI and EEG investigations compared to control groups.

To further explore potential thermal-related injuries to brain tissue around electrodes in patients that underwent simultaneous MRI and
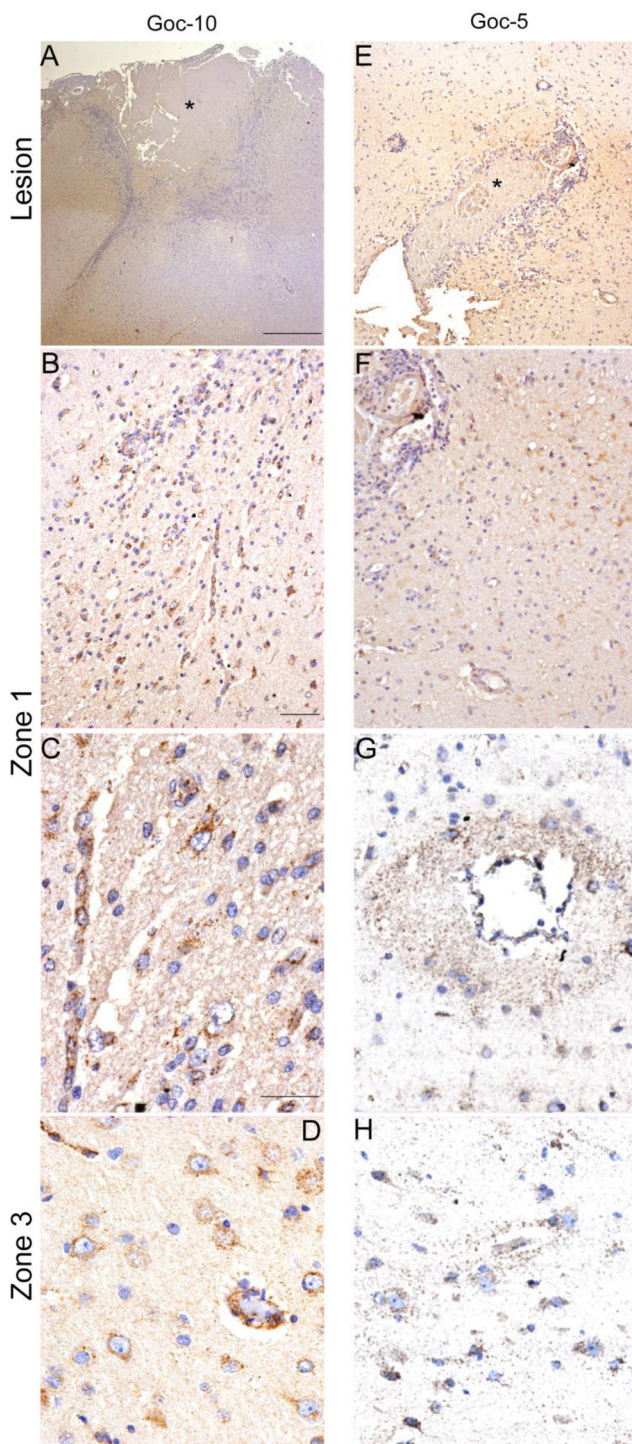
Fig. 4. HSP60-immunopositive labeling around the icEEG electrode penetrating injuries. Left (A,C,E,G): patient Goc-10 who had simultaneous icEEG-fMRI and structural MRI with icEEG electrodes; Right (B,D,F,H): patient Goc-5 who underwent structural MRI with icEEG electrodes in place only. The age of injury were 13 days and 10 days old, respectively. In both cases, HSP60-immunopositive labeling was strongly observed in neuronal, glial and endothelial-like cells near the injury (*) (zone 1; C-F), and less intensely in remote region, zone 3 (G-H). Granular HSP60-immunolabelling was often observed in the parenchyma around vascular structures near the injury (F). Scale in A: 1 mm; B: 200 μm; C, D: 100 μm; E-H: 50 μm.
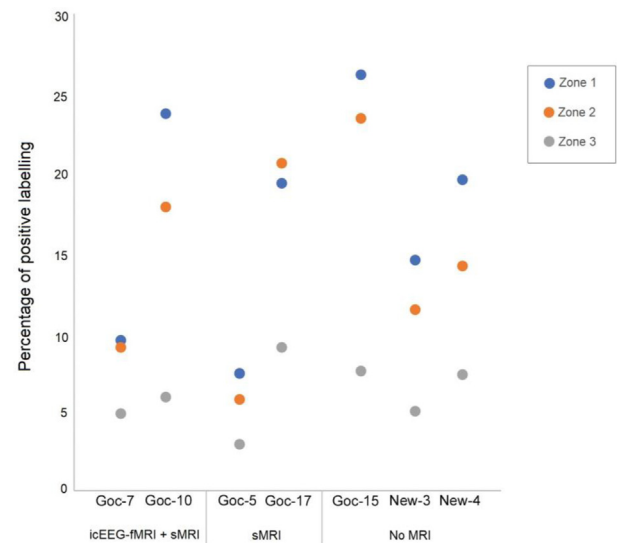

Fig. 5. Proportion of HSP60-immunopositive labeling. The patterns between regions near (zones 1 and 2) and remote (zone 3) from the icEEG electrode penetrating lesion are similar, across the seven cases studied using HSP60 and irrespective of exposure to MRI. Cases Goc-7 and Goc-10 underwent icEEG-fMRI and structural MRI (sMRI) with implanted icEEG electrodes; Goc-5 and Goc-17 underwent sMRI with implanted icEEG electrodes only; and Goc-15, New-3 and New-4 had no MRI with icEEG electrodes.

EEG, immunohistochemical investigation of heat shock proteins (HSP) were performed. HSP are inducible by thermal and oxidative stress and they maintain protein homeostasis through regulating protein folding and removal of misfolded aggregates during stress (Stetler et al., 2010). HSP60 is one of the most evolutionarily conserved HSP, and it is upregulated in response to heat shock as well as oxidative stress and DNA damage in the mammalian brain (D'Souza and Brown, 1998; Sarangi et al., 2013; Sharma et al., 2007). Little is known about HSP60 expression in the epileptic human brain; however, a previous study using limbic model of Temporal Lobe Epilepsy found elevated level of HSP60 in the hippocampus (including regions where stimulating and recording electrode placements were placed) of test and sham animals (with electrode placement but no stimulation) compared to control rats (Gammazza et al., 2015). In this study, HSP60 expression was higher in brain regions closer to the lesion compared to control (zone 3) but no remarkable changes were noted between groups.

The main limitations of this study are the following: First, this study contains a small number of patients due to the fact that these types of fMRI studies are rarely performed (with a total of 38 scans reported in the literature since 2011) and it is very difficult to obtain samples of the brain tissue post-icEEG implantations. The additional selection criterion of histopathology being available along the implanted depth electrodes' paths further increases the difficulty of collecting the kind of evidence we sought. This number is small because other patients either did not have icEEG electrodes or did not proceed to surgery or had surgery, but resections did not include brain regions in which icEEG electrodes were implanted. Second, while RF-induced heating damage may be spatially inhomogeneous, the same sampling procedure was followed as in (Goc et al., 2014), and therefore is limited to the immediate vicinity of the implanted electrodes. This is due to the focus of the ongoing study in our center on the impact of icEEG electrodes implantation on the surrounding tissue, and for which the tissue samples were collected (Goc et al., 2014). Therefore, we only investigated the expression of heat shock protein immediately around the area of injury. Also, while the extent of tract necrosis may be an indicator of the severity of injury, this was not quantified. Third, the pathological assessment presented here is an *ex vivo* assessment of resected materials, and other studies have reported pathological changes associated with icEEG (Fong et al., 2012).

It is unknown whether further brain damage takes place *in vivo*, as a result of invasive EEG to the brain of patients. However, according to our experience of imaging 19 patients implanted with icEEG using fMRI, no other complications have been observed or reported. Finally, spatial coverage provided by the pathology slices is incomplete and therefore some damage may have been missed. In particular, it is possible that the slices did not capture possible damage due to their specific orientation in relation to the electrode trajectories. We hope that this work may encourage other studies of existing tissue samples from subjects who underwent MRI with implants.

While this investigation is not a substitute for preparatory safety evaluations (as were performed previously to the present data being acquired (Carmichael et al., 2010, 2012)), we suggest that data derived from human *in-vivo* experiments *following* prospective evaluation such as presented here is rare and valuable. Furthermore, phantom tests and/or computational simulations such as those recommended for off-label use (as was the case for the acquisition of the MRI data described here), or legally required for device commercialization regulatory approval (e.g. FDA), have their own limitations – they are models of very complex systems that require validation. In this context we believe that this work, despite its limitations in terms of sample size and generalization, provides a methodology and concrete and particularly direct evidence relevant to this issue, and might encourage others to undertake similar studies prospectively, at the earliest possible opportunity.

In conclusion, despite the limitations of MRI safety testing in phantoms that lead us to perform functional MRI in the presence of implanted EEG electrodes, we now provide histopathological and heat shock protein expression evidence to the effect that following our strict protocol, as performed in our center at 1.5T using our low-SAR ($\leq$0.1 W/kg) scanning protocol and head transmit RF coil (Carmichael et al., 2012) did not result in significant additional brain damage in the cases studied. While it is not possible to generalize the results of our study, we believe that our methodology constitutes a useful framework for the post-hoc monitoring of MR scanning in the presence of brain implants, and could, in the hands of other investigators, provide a growing body of empirical evidence against which the traditional preparatory safety assessment work (i.e. theoretical, and phantom and computational experiments) should be assessed.

Data and code availability statement

The data described in this work cannot be made openly available due to ethical and privacy issues of clinical data.

Credit authorship contribution statement

Joan Y.W. Liu: Conceptualization, Methodology, Data curation, Writing – original draft, Visualization, Investigation, Writing – review & editing. **Hassan B. Hawsawi:** Writing – original draft, Writing – review & editing. **Niraj Sharma:** Methodology, Data curation, Writing – review & editing. **David W. Carmichael:** Writing – review & editing. **Beate Diehl:** Visualization, Investigation, Writing – review & editing. **Maria Thom:** Methodology, Data curation, Supervision, Writing – review & editing. **Louis Lemieux:** Conceptualization, Supervision, Writing – review & editing.

Acknowledgments

Appendix: Details of the icEEG electrode implantations

Patient Goc-5 (sMRI only) underwent the following implantation of four electrodes:

- Two 6-contact depth electrodes (Ad-Tech electrode type SD06R-SP05X) were inserted, one into left amygdala and labeled LA1 to LA6 and the other into left hippocampus and labeled LH1 to LH6 (spacing: 5 mm);
- One 32-contact subdural grid (Ad-Tech electrode type FG32A-SP10X) was placed over the left lateral temporal lobe, mostly infra-sylvian in such a way that contact number 1 was oriented in the anterior/superior position whilst the last contact number 32 was oriented in the posterior/inferior position. The grid positions were labeled G1 to G32 (spacing: 10 mm);
- One subdural strip with 6 contacts (Ad-Tech electrode type MS06R-IP10X-0JH) was placed as a unilateral implantation in the left basal temporal region (close to contact G29). The strip contacts were labeled AT1 to AT6 (spacing: 10 mm).

Patient Goc-7 (icEEG-fMRI and sMRI) underwent the following implantation of six electrodes:

- Two depth electrodes: a 6-contact (Ad-Tech type SD06R-SP05X) inserted in the left frontal lobe and labeled as DA.01 to DA.06 and a 4-contact (Ad-Tech type SD04R-SP05X) inserted posterior to DA in the left frontal lobe and with contacts labeled DP.01 to DP.04 (spacing: 5 mm);
- Two subdural grids: one 8 × 8-contact grid (Ad-Tech electrode type FG64C-SP10X-0C6) placed in the left frontal lobe; contacts labeled G1.01 to G1.64; and a 2 × 8 contact grid (Ad-Tech electrode type FG16A-SP10X) implanted sub frontally; with contacts labeled G2.01 to G2.16 (spacing: 10 mm);
- Two 6-contact subdural strips (Ad-Tech type IS06R-IP10X-0JH) were placed over the left frontal pole with contacts labeled S1.01 to S1.06 and S2.01 to S2.06, respectively (spacing: 10 mm).

Patient Goc-10 (icEEG-fMRI and sMRI) had four implanted electrodes:

- Two 4-contact depth electrodes (Ad-Tech type SD04R-SP05X) inserted in the left superior frontal sulcus; labeled DA-01 to DA-04 and DP-01 to DP-4, respectively (spacing: 5 mm);
- One 8 × 8 contacts subdural grid (Ad-Tech type FG64C-SP10X-0C6) placed in the left lateral frontal region, covering the superior and middle parts of the inferior frontal gyrus, pre-central gyrus, central sulcus and part of the post-central sulcus; contacts labeled G1-01 to G1-64 (spacing: 10 mm);
- One 2 × 8 contacts subdural grid (Ad-Tech type FG16A-SP10X) positioned in the left parieto-temporal and post-central regions; with contacts labeled G2-01 to G2-16 (spacing: 10 mm).

Patient Goc-15 (no sMRI or icEEG-fMRI) had three implanted electrodes:

- One 6-contact depth electrode (Ad-Tech type SD06R-SP05X) was placed through the grid (see below) into the left frontal region and labeled D1 to D6 (spacing: 5 mm);
- One 48-contact subdural grid electrode (Ad-Tech type FG48G-SS10X-000) was placed over the left frontal region; contacts labeled G1-G48 (spacing: 10 mm);
- One 6-contact subdural strip (Ad-Tech) was placed over the left parietal region; contacts labeled S1-S6 (spacing: 10 mm).

Patient Goc-17 (sMRI only) had five implanted electrodes:

- Four 6-contact depth electrodes (Ad-Tech type SD06R-SP05X) were implanted to target each of the following structures: the right

amygdala, right hippocampus, left amygdala and left hippocampus; contacts labeled RA1-RA6, RH1-RH6, LA1-LA6, LH1-LH6 (spacing: 5 mm);

One 6-contact subdural strip (Ad-Tech) was placed over the right frontal region; contacts labelled S1-S7 (spacing: 10 mm).

Patient NEW-1 (icEEG-fMRI and sMRI) had four implanted electrodes:

Two 6-contact depth electrodes (Ad-Tech type SD04R-SP05X) targeting the left amygdala and hippocampus; contacts labelled LA1-LA6 and LH1-LH6 (spacing: 5 mm for the 3 deepest contacts and 10 mm for the 3 most superficial);

One 4 × 8 contacts subdural grid (Ad-Tech type FG32A-SP10X), partially covering the left lateral temporal lobe and part of the frontal lobe, labeled (GA). The most anterior inferior contact was GA-01 and the most anterior superior contact was GA-25. The most posterior inferior contact was GA-08 and the most posterior superior contact was GA-32 (spacing: 10 mm);

One 4 × 8 contacts subdural grid (Ad-Tech type FG32A-SP05X) covering the left basal temporal lobe. The most lateral anterior contact was GB32, and the most mesial posterior was GB-01 (spacing: 5 mm).

Patient NEW-2 (sMRI only) had eight implanted electrodes:

Three 6-contact depth electrodes were inserted (all Ad-Tech type SD06R-SP10X) (all spacing: 10 mm): one targeting the left amygdala through a hole made between GA20 and GA12, and labelled AM1-AM6. A second targeting the anterior hippocampus was inserted between GA21, GA22, GA29 and GA30, and labeled AH1-AH6. The third targeted the posterior hippocampus, and was inserted between GA31 and GA32 and labeled PH1-PH6;

A fourth depth electrode, with 10 contacts (Ad-Tech type SD06R-SP05X), was inserted into the left Heschel's gyrus between GA14, GA15, GA22 and GA23 and labelled HG1-HG6 (spacing: 5 mm);

Two subdural grids: one with 32 contacts (Ad-Tech type FG32A-SP100X), placed over the lateral temporal lobe, labeled GA01-GA32 (spacing: 10 mm). The second had 24 contacts (Ad-Tech type FG24A-SP05X) positioned over the left basal temporal area and labeled GB01-GB24 (spacing: 5 mm);

Two subdural strips were placed. One strip 6-contact strip (Ad-Tech type IS06R-IP10X-0JH) in the left superior Sylvian area, positioned such that contact number 6 was adjacent to GA06, and the contacts were labelled SS1-SS6 (spacing: 10 mm). The second 6-contact strip (Ad-Tech type MS06R-IP10X-0JH) was positioned in the sub frontal area such that contact 6 was close to GA06; and the contacts were labeled SF1-SF6 (spacing: 10 mm).

Patient NEW-3 (no sMRI or icEEG-fMRI) had four implanted electrodes:

One 48-contact subdural grid electrode (Ad-Tech type FG48G-SS10X-000) was placed over the left frontal region; contacts labeled GA1-GA48 (spacing: 10 mm);

One 32-channel subdural grid (Ad-Tech type FG32A-SP100X) was over the inferior aspect of the left frontal lobe; contacts labeled GB1-GB32 (spacing: 10 mm);

Two 6-contact subdural strips (Ad-Tech type IS06R-IP10X-0JH) were placed over the left anterior frontal region; contacts labeled F1-F6 and FP1-FP6 (spacing: 10 mm).

Patient NEW-4 (no sMRI or icEEG-fMRI) had six implanted electrodes:

Two 6-contact depth electrodes (Ad-Tech type SD04R-SP05X) were inserted in the left frontal lobe and labeled DA01-DA06 and DP01-DP06 (spacing: 5 mm for the 3 deepest contacts and 10 mm for the 3 most superficial);

One 48-contact subdural grid electrode (Ad-Tech type FG48G-SS10X-000) was placed over the left frontal region; contacts labeled GA1-GA48 (spacing: 10 mm);

One 4 × 4 grid (Ad-Tech) was placed over the mesial aspect of the left frontal lobe; contacts labelled GB1-GB16 (spacing: 10 mm);

Two 6-contact subdural strips (Ad-Tech type IS06R-IP10X-0JH) were placed over the fronto-parietal convexity; contacts labelled SA1-SA6 and SB1-SB6 (spacing: 10 mm).

References

An, D., Fahoum, F., Hall, J., Olivier, A., Gotman, J., Dubeau, F., 2013. Electroencephalography/functional magnetic resonance imaging responses help predict surgical outcome in focal epilepsy. Epilepsia 54, 2184–2194. doi:10.1111/epi.12434.

Angelone, L.M., Potthast, A., Segonne, F., Iwaki, S., Belliveau, J.W., Bonmassar, G., 2004. Metallic electrodes and leads in simultaneous EEG-MRI: specific absorption rate (SAR) simulation studies. Bioelectromagnetics doi:10.1002/bem.10198.

Angelone, L.M., Vasios, C.E., Wiggins, G., Purdon, P.L., Bonmassar, G., 2006. On the effect of resistive EEG electrodes and leads during 7 T MRI: simulation and temperature measurement studies. Magn. Reson. Imaging doi:10.1016/j.mri.2006.01.006.

ANSI-AAMI-ISO-14708, 2012. Implants for surgery-Active implantable medical devices-part 3: implantable neurostimulators. SMPTE J. 95, 601–602. doi:10.5594/j17740.

Bankhead, P., Loughrey, M.B., Fernández, J.A., Dombrowski, Y., McArt, D.G., Dunne, P.D., McQuaid, S., Gray, R.T., Murray, L.J., Coleman, H.G., James, J.A., Salto-Tellez, M., Hamilton, P.W., 2017. QuPath: open source software for digital pathology image analysis. Sci. Rep. 7, 16878. doi:10.1038/s41598-017-17204-5.

Blümcke, I., Thom, M., Aronica, E., Armstrong, D.D., Vinters, H.V., Palmini, A., Jacques, T.S., Avanzini, G., Barkovich, A.J., Battaglia, G., Becker, A., Cepeda, C., Cendes, F., Colombo, N., Crino, P., Cross, J.H., Delalande, O., Dubeau, F., Duncan, J., Guerrini, R., Kahane, P., Mathern, G., Najm, I., Özkara, Ç., Raybaud, C., Represa, A., Roper, S.N., Salamon, N., Schulze-Bonhage, A., Tassi, L., Vezzani, A., Spreafico, R., 2011. The clinicopathologic spectrum of focal cortical dysplasias: a consensus classification proposed by an ad hoc task force of the ILAE diagnostic methods commission. Epilepsia 52, 158–174. doi:10.1111/j.1528-1167.2010.02777.x.

Carmichael, D.W., Pinto, S., Limousin-Dowsey, P., Thobois, S., Allen, P.J., Lemieux, L., Yousry, T., Thornton, J.S., 2007. Functional MRI with active, fully implanted, deep brain stimulation systems: safety and experimental confounds. doi:10.1016/j.neuroimage.2007.04.058.

Carmichael, D.W., Thornton, J.S., Rodionov, R., Thornton, R., McEvoy, A., Allen, P.J., Lemieux, L., 2008. Safety of localizing epilepsy monitoring intracranial electroencephalograph electrodes using MRI: radiofrequency-induced heating. J. Magn. Reson. Imaging 28, 1233–1244. doi:10.1002/jmri.21583.

Carmichael, D.W., Thornton, J.S., Rodionov, R., Thornton, R., McEvoy, A.W., Ordidge, R.J., Allen, P.J., Lemieux, L., 2010. Feasibility of simultaneous intracranial EEG-fMRI in humans: a safety study. Neuroimage 49, 379–390. doi:10.1016/j.neuroimage.2009.07.062.

Carmichael, D.W., Vulliemoz, S., Rodionov, R., Thornton, J.S., Mcevoy, A.W., Lemieux, L., 2012. Simultaneous intracranial EEG-fMRI in humans: protocol considerations and data quality. Neuroimage 63, 301–309. doi:10.1016/j.neuroimage.2012.05.056.

Centeno, M., Tierney, T.M., Perani, S., Shamshiri, E.A., StPier, K., Wilkinson, C., Konn, D., Vulliemoz, S., Grouiller, F., Lemieux, L., Pressler, R.M., Clark, C.A., Helen Cross, J., Carmichael, D.W., 2017. Combined EEG-fMRI and ESI improves localisation of paediatric focal epilepsy. Ann. Neurol. 2–30. doi:10.1002/ana.25003.

Chaudhary, U.J., Centeno, M., Thornton, R.C., Rodionov, R., Vulliemoz, S., McEvoy, A.W., Diehl, B., Walker, M.C., Duncan, J.S., Carmichael, D.W., Lemieux, L., 2016. Mapping human preictal and ictal haemodynamic networks using simultaneous intracranial EEG-fMRI. NeuroImage Clin. 11, 486–493. doi:10.1016/j.nicl.2016.03.010.

Coan, A.C., Chaudhary, U.J., Grouiller, F., Campos, B.M., Perani, S., De Ciantis, A., Vulliemoz, S., Diehl, B., Beltramini, G.C., Carmichael, D.W., Thornton, R.C., Covolan, R.J., Cendes, F., Lemieux, L., 2016. EEG-fMRI in the presurgical evaluation of temporal lobe epilepsy. J. Neurol. Neurosurg. Psychiatry 87, 642–649. doi:10.1136/jnnp-2015-310401.

Coffey, R.J., Kalin, R., Olsen, J.M., 2014. Magnetic resonance imaging conditionally safe neurostimulation leads: investigation of the maximum safe lead tip temperature. Neurosurgery 74, 215–225. doi:10.1227/NEU.0000000000000242.

Cunningham, C.B.J., Goodyear, B.G., Badawy, R., Zaamout, F., Pittman, D.J., Beers, C.A., Federico, P., 2012. Intracranial EEG-fMRI analysis of focal epileptiform discharges in humans 53, 1636–1648. doi:10.1111/j.1528-1167.2012.03601.x.

D'Souza, S.M., Brown, I.R., 1998. Constitutive expression of heat shock proteins Hsp90, Hsc70, Hsp70 and Hsp60 in neural and non-neural tissues of the rat during postnatal development. Cell Stress Chaperones 3, 188–199 10.1379/1466-1268(1998)003<0188:ceohsp>2.3.co;2.

Davis, L.M., Spencer, D.D., Spencer, S.S., Bronen, R.A., 1999. MR imaging of implanted depth and subdural electrodes: is it safe? Epilepsy Res. 35, 95–98. doi:10.1016/S0920-1211(99)00007-8.

Deichmann, R., 2016. Principles of MRI and Functional MRI. In: Filippi, M. (Ed.), fMRI Techniques and Protocols. Humana Press, New York, NY, pp. 3–28. doi:10.1007/978-1-4939-5611-1_1.

Enatsu, R., Mikuni, N., 2016. Invasive evaluations for epilepsy surgery: a review of the literature. Neurol. Med. Chir. 56, 221–227. doi:10.2176/nmc.ra.2015-0319, (Tokyo).

Erhardt, J.B., Fuhrer, E., Gruschke, O.G., Leupold, J., Wapler, M.C., Hennig, J., Stieglitz, T., Korvink, J.G., 2018. Should patients with brain implants undergo MRI? J. Neural Eng. 15. doi:10.1088/1741-2552/aab4e4.

Fong, J.S., Alexopoulos, A.V., Bingaman, W.E., Gonzalez-Martinez, J., Prayson, R.A., 2012. Pathologic findings associated with invasive EEG monitoring for medically intractable epilepsy. Am. J. Clin. Pathol. 138, 506–510. doi:10.1309/AJCPGSNL9VDVNJMX.

Gammazza, A.M., Colangeli, R., Orban, G., Pierucci, M., Di Gennaro, G., Bello, M.Lo, D'Aniello, A., Bucchieri, F., Pomara, C., Valentino, M., Muscat, R., Benigno, A., Zummo, G., de Macario, E.C., Cappello, F., Di Giovanni, G., Macario, A.J.L., 2015. Hsp60 response in experimental and human temporal lobe epilepsy. Sci. Rep. 5, 9434. doi:10.1038/srep09434.

Glynn, S.M., Detre, J.A., 2013. Imaging epilepsy and epileptic seizures using fMRI. In: Ulmer, S., Jansen, O. (Eds.), fMRI: basics and clinical applications. Springer Berlin Heidelberg, Berlin, Heidelberg, pp. 177–189. doi:10.1007/978-3-642-34342-1_14.

Goc, J., Liu, J.Y.W., Sisodiya, S.M., Thom, M., 2014. A spatiotemporal study of gliosis in relation to depth electrode tracks in drug-resistant epilepsy. Eur. J. Neurosci. 39, 2151–2162. doi:10.1111/ejn.12548.

Goebel, R., Esposito, F., 2010. The added value of EEG–fMRI in imaging neuroscience. In: Mulert, C., Lemieux, L. (Eds.), EEG - fMRI. Springer Berlin Heidelberg, Berlin, Heidelberg, pp. 97–112. doi:10.1007/978-3-540-87919-0_6.

Golestanirad, L., Angelone, L.M., Iacono, M.I., Katnani, H., Wald, L.L., Bonmassar, G., 2017a. Local SAR near deep brain stimulation (DBS) electrodes at 64 and 127 MHz: a simulation study of the effect of extracranial loops. Magn. Reson. Med. 78, 1558–1565. doi:10.1002/mrm.26535.

Golestanirad, L., Keil, B., Angelone, L.M., Bonmassar, G., Mareyam, A., Wald, L.L., 2017b. Feasibility of using linearly polarized rotating birdcage transmitters and close-fitting receive arrays in MRI to reduce SAR in the vicinity of deep brain simulation implants. Magn. Reson. Med. doi:10.1002/mrm.26220.

Golestanirad, L., Kirsch, J., Bonmassar, G., Downs, S., Elahi, B., Martin, A., Iacono, M.I., Angelone, L.M., Keil, B., Wald, L.L., Pilitsis, J., 2019. RF-induced heating in tissue near bilateral DBS implants during MRI at 1.5 T and 3T: the role of surgical lead management. Neuroimage 184, 566–576. doi:10.1016/j.neuroimage.2018.09.034.

Gonzalez-Martinez, J., Bingaman, W., Chauvel, P., Najm, I., 2015. Straegies and indications for evaluation with invasive electrodes. In: Wyllie, E., Gidal, B., Goodkin, H., Loddenkemper, T., Sirven, J. (Eds.), Wyllie's Treatment of Epilepsy: Principles and Practice. Wolters Kluwer, Philadelphia.

Hawsawi, H.B., Carmichael, D.W., Lemieux, L., 2017. Safety of simultaneous scalp or intracranial EEG during MRI: a review. Frontiers in Physics 5, 42. doi:10.3389/fphy.2017.00042.

Jayakar, P., Gotman, J., Harvey, A.S., Palmini, A., Tassi, L., Schomer, D., Dubeau, F., Bartolomei, F., Yu, A., Kršek, P., Velis, D., Kahane, P., 2016. Diagnostic utility of invasive EEG for epilepsy surgery: indications, modalities, and techniques. Epilepsia 57, 1735–1747. doi:10.1111/epi.13515.

Koubeissi, M.Z., Puwanant, A., Jehi, L., Alshekhlee, A., 2009. In-hospital complications of epilepsy surgery: a six-year nationwide experience. Br. J. Neurosurg. 23, 524–529. doi:10.1080/02688690903019589.

Larson, P.S., Richardson, R.M., Starr, P.A., Martin, A.J., 2008. Magnetic resonance imaging of implanted deep brain stimulators: experience in a large series. Stereotact. Funct. Neurosurg. 86, 92–100. doi:10.1159/000112430.

Lemieux, L., Allen, P.J., Franconi, F., Symms, M.R., Fish, D.R., 1997. Recording of EEG during fMRI experiments: patient safety. Magn. Reson. Med. 38, 943–952. doi:10.1002/mrm.1910380614.

Liu, J.Y.W., Thom, M., Catarino, C.B., Martinian, L., Figarella-Branger, D., Bartolomei, F., Koepp, M., Sisodiya, S.M., 2012. Neuropathology of the blood-brain barrier and pharmaco-resistance in human epilepsy. Brain 135, 3115–3133. doi:10.1093/brain/aws147.

U.S. Food and Drug Administration (US-FDA). 2021. *Investigator Responsibilities – Safety Reporting for Investigational D.* [online] Available at: <https://www.fda.gov/regulatory-information/search-fda-guidance-documents/investigator-responsibilities-safety-reporting-investigational-drugs-and-devices>

IEC, 2016. Medical electrical equipment–Part 2-33: Particular requirements for the basic safety and essential performance of magnetic resonance equipment for medical diagnosis. International Electrotechnical Commission 60601-2-33:2010 + A12:2016, Geneva.

MHRA, 2015. Safety guidelines for magnetic resonance imaging equipment in clinical use. Medicines and Healthcare Products Regulatory Agency, London.

Murta, T., Chaudhary, U.J., Tierney, T.M., Dias, A., Leite, M., Carmichael, D.W., Figueiredo, P., Lemieux, L., 2017. Phase-amplitude coupling and the BOLD signal: a simultaneous intracranial EEG (icEEG) - fMRI study in humans performing a finger-tapping task. Neuroimage 146, 438–451. doi:10.1016/J.NEUROIMAGE.2016.08.036.

Murta, T., Figueiredo, P., Lemieux, L., Leite, M., Carmichael, D.W., 2014. Electrophysiological correlates of the BOLD signal for EEG-informed fMRI. Hum. Brain Mapp. 36, 391–414. doi:10.1002/hbm.22623.

Murta, T., Hu, L., Tierney, T.M., Chaudhary, U.J., Walker, M.C., Carmichael, D.W., Figueiredo, P., Lemieux, L., 2016. A study of the electro-haemodynamic coupling using simultaneously acquired intracranial EEG and fMRI data in humans. Neuroimage 142, 371–380. doi:10.1016/J.NEUROIMAGE.2016.08.001.

Nazzaro, J.M., Lyons, K.E., Wetzel, L.H., Pahwa, R., 2010. Use of brain MRI after deep brain stimulation hardware implantation. Int. J. Neurosci. 120, 176–183. doi:10.3109/00207450903389156.

Oya, H., Howard, M.A., Magnotta, V.A., Kruger, A., Griffiths, T.D., Lemieux, L., Carmichael, D.W., Petkov, C.I., Kawasaki, H., Kovach, C.K., Sutterer, M.J., Adolphs, R., 2017. Mapping effective connectivity in the human brain with concurrent intracranial electrical stimulation and BOLD-fMRI. J. Neurosci. Methods 277, 101–112. doi:10.1016/j.jneumeth.2016.12.014.

Reeves, C., Pradim-Jardim, A., Sisodiya, S.M., Thom, M., Liu, J.Y.W., 2019. Spatiotemporal dynamics of PDGFRβ expression in pericytes and glial scar formation in penetrating brain injuries in adults. Neuropathol. Appl. Neurobiol. 45, 609–627. doi:10.1111/nan.12539.

Ridley, B., Wirsich, J., Bettus, G., Rodionov, R., Murta, T., Chaudhary, U., Carmichael, D., Thornton, R., Vulliemoz, S., McEvoy, A., Wendling, F., Bartolomei, F., Ranjeva, J.-P., Lemieux, L., Guye, M., 2017. Simultaneous intracranial EEG-fMRI shows inter-modality correlation in time-resolved connectivity within normal areas but not within epileptic regions. Brain Topogr. 30, 639–655.

Sapareto, S.A., Dewey, W.C., 1984. Thermal dose determination in cancer therapy. Int. J. Radiat. Oncol. Biol. Phys. 10, 787–800. doi:10.1016/0360-3016(84)90379-1.

Sarangi, U., Singh, M.K., Abhijnya, K.V.V., Reddy, L.P.A., Prasad, B.S., Pitke, V.V., Paithankar, K., Sreedhar, A.S., 2013. Hsp60 chaperonin acts as barrier to pharmacologically induced oxidative stress mediated apoptosis in tumor cells with differential stress response. Drug Target Insights 7. doi:10.4137/DTI.S12513, DTI.S12513.

Serano, P., Angelone, L.M., Katnani, H., Eskandar, E., Bonmassar, G., 2015. A novel brain stimulation technology provides compatibility with MRI. Sci. Rep. doi:10.1038/srep09805.

Sharma, S., Rohilla, M.S., Tiwari, P.K., 2007. Developmental and hyperthermia-induced expression of the heat shock proteins HSP60 and HSP70 in tissues of the housefly Musca domestica: an *in vitro* study. Genet. Mol. Biol. 30, 159–168.

Stephan, C.L., Kepes, J.J., Santacruz, K., Wilkinson, S.B., Fegley, B., Osorio, I., 2001. Spectrum of clinical and histopathologic responses to intracranial electrodes: from multifocal aseptic meningitis to multifocal hypersensitivity-type meningovasculitis. Epilepsia 42, 895–901. doi:10.1046/j.1528-1157.2001.042007895.x.

Stetler, R.A., Gan, Y., Zhang, W., Liou, A.K., Gao, Y., Cao, G., Chen, J., 2010. Heat shock proteins: cellular and molecular mechanisms in the central nervous system. Prog. Neurobiol. 92, 184–211. doi:10.1016/j.pneurobio.2010.05.002.

Tao, J.X., Ray, A., Hawes-Ebersole, S., Ebersole, J.S., 2005. Intracranial EEG substrates of scalp EEG interictal spikes. Epilepsia 46 (5), 669–676.

Thornton, R., Laufs, H., Rodionov, R., Cannadathu, S., Carmichael, D.W., Vulliemoz, S., Salek-Haddadi, A., McEvoy, A.W., Smith, S.M., Lhatoo, S., Elwes, R.D.C., Guye, M., Walker, M.C., Lemieux, L., Duncan, J.S., 2010. EEG correlated functional MRI and postoperative outcome in focal epilepsy. J. Neurol. Neurosurg. Psychiatry 81, 922–927. doi:10.1136/jnnp.2009.196253.

Van Eden, W., Van Der Zee, R., Prakken, B., 2005. Heat-shock proteins induce T-cell regulation of chronic inflammation. Nat. Rev. Immunol. 5, 318–330. doi:10.1038/nri1593.

Vulliemoz, S., Diehl, B., Walker, M.C., Rosenkranz, K., Rodionov, R., McEvoy, A.W., Carmichael, D.W., Lemieux, L., 2011. Simultaneous intracranial EEG and fMRI of interictal epileptic discharges in humans. Neuroimage 54, 182–190. doi:10.1016/j.neuroimage.2010.08.004.

Vulliemoz, S., Lemieux, L., Daunizeau, J., Michel, C.M., Duncan, J.S., 2010. The combination of EEG source imaging and EEG-correlated functional MRI to map epileptic networks. Epilepsia 51, 491–505. doi:10.1111/j.1528-1167.2009.02342.x.

Weise, L.M., Schneider, G.H., Kupsch, A., Haumesser, J., Hoffmann, K.T., 2010. Postoperative MRI examinations in patients treated by deep brain stimulation using a non-standard protocol. Acta Neurochir. 152, 2021–2027. doi:10.1007/s00701-010-0738-y, (Wien).

Yan, H., Katz, J.S., Anderson, M., Mansouri, A., Remick, M., Ibrahim, G.M., Abel, T.J., 2019. Method of invasive monitoring in epilepsy surgery and seizure freedom and morbidity: a systematic review. Epilepsia 60, 1960–1972. doi:10.1111/epi.16315.

Zrinzo, L., Yoshida, F., Hariz, M.I., Thornton, J., Foltynie, T., Yousry, T.A., Limousin, P., 2011. Clinical safety of brain magnetic resonance imaging with implanted deep brain stimulation hardware: large case series and review of the literature. World Neurosurg. 76, 164–172. doi:10.1016/j.wneu.2011.02.029.